

# Earth and Space Science



### RESEARCH ARTICLE

10.1029/2023EA003143

### **Key Points:**

- The detection performance of Guangdong Lightning Mapping Array has been evaluated using Monte Carlo and an aircraft track, and both methods showed good consistency
- Location errors over the network are within 18 m horizontally and 50 m vertically, when outside the network they show directionality
- Very high frequency (VHF) and low frequency lightning location results are similar, but VHF sources are more located ahead along the channel

#### Correspondence to:

Y. Zhang, zhangyang@cma.gov.cn

#### Citation:

Zhang, H., Zhang, Y., Fan, Y., Zhang, Y., Krehbiel, P. R., & Lyu, W. (2023). Guangdong Lightning Mapping Array: Errors evaluation and preliminary results. *Earth and Space Science*, 10, e2023EA003143. https://doi.org/10.1029/2023EA003143

Received 29 JUN 2023 Accepted 10 OCT 2023

#### **Author Contributions:**

Investigation: Huivi Zhang

Conceptualization: Yang Zhang Data curation: Huiyi Zhang, Yang Zhang, Yanfeng Fan Formal analysis: Huiyi Zhang, Yang Zhang

Methodology: Huiyi Zhang, Yang Zhang Project Administration: Yang Zhang Resources: Yang Zhang, Yanfeng Fan, Paul R. Krehbiel

Supervision: Yang Zhang, Yijun Zhang, Paul R. Krehbiel, Weitao Lyu Visualization: Huiyi Zhang Writing – original draft: Huiyi Zhang,

Yang Zhang
Writing – review & editing: Huiyi
Zhang, Yang Zhang

# © 2023 The Authors.

This is an open access article under the terms of the Creative Commons Attribution-NonCommercial License, which permits use, distribution and reproduction in any medium, provided the original work is properly cited and is not used for commercial purposes.

# **Guangdong Lightning Mapping Array: Errors Evaluation and Preliminary Results**

Huiyi Zhang<sup>1</sup>, Yang Zhang<sup>1</sup>, Yanfeng Fan<sup>1</sup>, Yijun Zhang<sup>2</sup>, Paul R. Krehbiel<sup>3</sup>, and Weitao Lyu<sup>1</sup>

<sup>1</sup>State Key Laboratory of Severe Weather, Chinese Academy of Meteorological Sciences, Beijing, China, <sup>2</sup>Department of Atmospheric and Oceanic Sciences, Institute of Atmospheric Sciences, Fudan University, Shanghai, China, <sup>3</sup>Langmuir Laboratory for Atmospheric Research, Geophysical Research Center, New Mexico Institute of Mining and Technology, Socorro, NM, USA

**Abstract** The Guangdong Lightning Mapping Array (GDLMA), as the first LMA in China, was deployed in Guangzhou, Guangdong Province, China, in November 2018 by the Chinese Academy of Meteorological Sciences and New Mexico Institute of Mining and Technology. An evaluation was conducted using Monte Carlo and an aircraft track. The average timing uncertainty of GDLMA is 35 ns based on the distributions of reduced chi-square values. Based on the aircraft track, the average horizontal error is 13 m and the average vertical error is 41 m at an altitude of 4–5 km over the network, consistent with the Monte Carlo results. Location errors outside the network exhibit noticeable directionality. The ability to characterize lightning channels varies with different location errors. In locations that are far from the network center, only the basic structure of lightning flash can be presented, while closer to the network, the flash channel structure can be mapped well. Compared with Low-to-Mid Frequency E-field Detection Array (MLFEDA), they were generally similar in overall structure, and some lightning flash characteristics such as flash duration and coverage area exhibited consistency. However, GDLMA demonstrated better flash channel structure characterization capability, while MLFEDA performed better in processes such as leader/return strokes. In addition, based on the comparison of spatial positions of one-on-one discharge events, we found that very high frequency sources were more located ahead of low frequency sources in the direction of lightning channel development.

### 1. Introduction

Lightning discharges are always accompanied by very high frequency (VHF) signals. Location techniques used in VHF detection networks include time of arrival (TOA) location technology and interferometer location technology. The Lightning Mapping Array (LMA) is a widely recognized TOA system developed by the New Mexico Institute of Mining and Technology (NMT) in the United States (Krehbiel et al., 2000; Rison et al., 1999; Thomas et al., 2004), possessing high three-dimensional (3D) lighting flash channel location accuracy. The LMA typically operates at 60–66 MHz, with each station using a Global Positioning System (GPS) receiver to record the peak time of radiation events that exceed a noise threshold in an 80 μs time window. Since its introduction in 1998, LMA has proven to be a useful tool in advancing our understanding of atmospheric electricity and has resulted in numerous significant discoveries. For example, it has helped reveal the storm charge structures and lightning activity characteristics in different terrains and storm types (Pineda et al., 2016; Rust et al., 2005; Salvador et al., 2021; Wiens et al., 2005; Zheng et al., 2019), investigate the cloud dynamics and microphysical configurations associated with lightning discharges (Bruning & MacGorman, 2013; Lang & Rutledge, 2008; Souza & Bruning, 2021; Tessendorf, 2007), and explore the relationship between aerosols and lightning activity (Barth et al., 2015; Carey et al., 2016; Davis et al., 2019).

Currently, LMAs have been deployed and applied in the United States, Brazil, Europe, Japan, and more. However, regional characteristics, deployment methods, equipment parameters, and other factors lead to variations in the actual detection performance of LMAs in different regions. It is necessary to evaluate the location accuracy and establish the effective detection range of the LMA before performing any analysis. Koshak et al. (2004) developed a comprehensive source retrieval algorithm and used Monte Carlo to analyze the location error of the North Alabama LMA, visually demonstrating the spatial distribution of errors. The average location uncertainty is within 50 m when VHF sources are within or near the network. Thomas et al. (2004) conducted a thorough evaluation of the New Mexico Tech LMA using sounding balloons equipped with a GPS receiver and VHF transmitter,

ZHANG ET AL. 1 of 16

a simple geometric model, and aircraft tracks. The evaluation results indicated that the positioning accuracy over the network is high, with a location uncertainty of 6–12 m in the horizontal direction and 20–30 m in the vertical direction. When outside the network, the location uncertainties increase with distance. Cullen (2013) evaluated the performance of Houston LMA based on the method proposed by Thomas et al. Chmielewski and Bruning (2016) further optimized the Monte Carlo model and evaluated of LMAs in four different regions in the United States. They found that the configuration and station receive thresholds highly affect LMA location errors and detection efficiency. For all networks within 100 km, the predicted flash detection efficiency exceeded 95%, and these flashes exhibited larger distortions at greater distances.

Before 2018, Chinese lightning researchers drew on LMA technology and initially developed VHF lightning 3D positioning systems (Zhang et al., 2010, 2015). However, there were certain differences in the performance of thunderstorm monitoring and lightning channel depiction compared to the LMA. To further assist the research on atmospheric electricity in China, the lightning detection group of the Chinese Academy of Meteorological Sciences (CAMS) introduced the LMA system from the NMT in November 2018. It was deployed at the Field Experiment Base on Lightning Sciences, China Meteorological Administration (CMA\_FEBLS) in Guangzhou, Guangdong Province, forming the GDLMA. The establishment of GDLMA is particularly useful for the study of thunderstorm electrification in Guangdong as the region is climatologically susceptible to thunderstorm activity.

Although GDLMA shows generally consistent with other measurement results, a detailed evaluation of the network's detection performance has not been conducted. In this study, the location errors of the network were evaluated employing a combination of theoretical methods and actual observation data obtained during experimental operations. This study can serve as a reference for effectively using GDLMA data. Lightning flash examples and an analysis of a multicell thunderstorm are also presented to show actual detection results. Furthermore, we compared the mapping results of GDLMA with the nearby deployed Low-to-Mid Frequency E-field Detection Array (MLFEDA), demonstrating the similarities and differences in their location performance.

#### 2. Station Network and Methods

# 2.1. **GDLMA**

The distribution of GDLMA stations is shown in Figure 1a, and the exterior view of a single station is shown in Figure 1b. When GDLMA was initially deployed in November 2018, there were nine stations with 6 MHz bandwidth receivers at a center frequency of 193 MHz. In August 2020, six stations were added around the triggered lightning experiments site for triggered lightning observations, with 6 MHz bandwidth receivers at a center frequency of 63 MHz. In 2021, 12 stations were conducting continuous observations, with baseline ranging from 2 to 43 km. The location error analysis primarily focused on the layout of the 12 stations. These stations employed a combination of two reception frequency bands, as indicated by the red and blue triangular markers in Figure 1a.

Since LMA has been specifically described (Fuchs et al., 2016; Koshak et al., 2004; Krehbiel et al., 2000; Rison et al., 1999; Thomas et al., 2004), only the relevant parameter settings and localization algorithm involved in the evaluation are briefly introduced. The lightning signals are digitized using a 25 MHz digital converter, and the arrival times of the highest VHF pulses are independently measured and recorded in 80  $\mu$ s time windows. Lightning radiation sources are located using the TOA method shown in Equation 1, where (x, y, z, t) is the spatiotemporal coordinates of a radiation source,  $(x_i, y_i, z_i, t_i)$  is the location and arrival time of station i and c is the signal propagation speed. Reduced chi-square  $(\chi^2_v)$  is an indicator that measures the goodness of fit between the observed arrival time matrix and the predicted arrival time solution matrix for each station sensor, as shown in Equation 2. The variable n is the number of stations participating in the solution,  $\nu = n - 4$  is the degrees of freedom,  $\Delta t_{rms}$  is timing uncertainty,  $t_i^{obs}$  is the arrival time measured by station i, and  $t_i^{fi}$  is the predicted arrival time obtained through Equation 1. The initial  $\Delta t_{rms}$  for GDLMA is 70 ns, and the actual  $\Delta t_{rms}$  can be estimated base on the  $\chi^2_v$  distributions of processed data.

$$t_i = t + \frac{1}{c}\sqrt{(x_i - x)^2 + (y_i - y)^2 + (z_i - z)^2}$$
 (1)

$$\chi_{\nu}^{2} = \sum_{i=1}^{N} \frac{\left(t_{i}^{\text{obs}} - t_{i}^{\text{fit}}\right)^{2}}{\Delta t_{\text{rms}}(n-4)}$$
 (2)

ZHANG ET AL. 2 of 16

onlinelibrary.wiley.com/doi/10.1029/2023EA003143 by New Mexico Institute Of Mining And Technology, Wiley Online Library on [19/07/2024]. See the Term

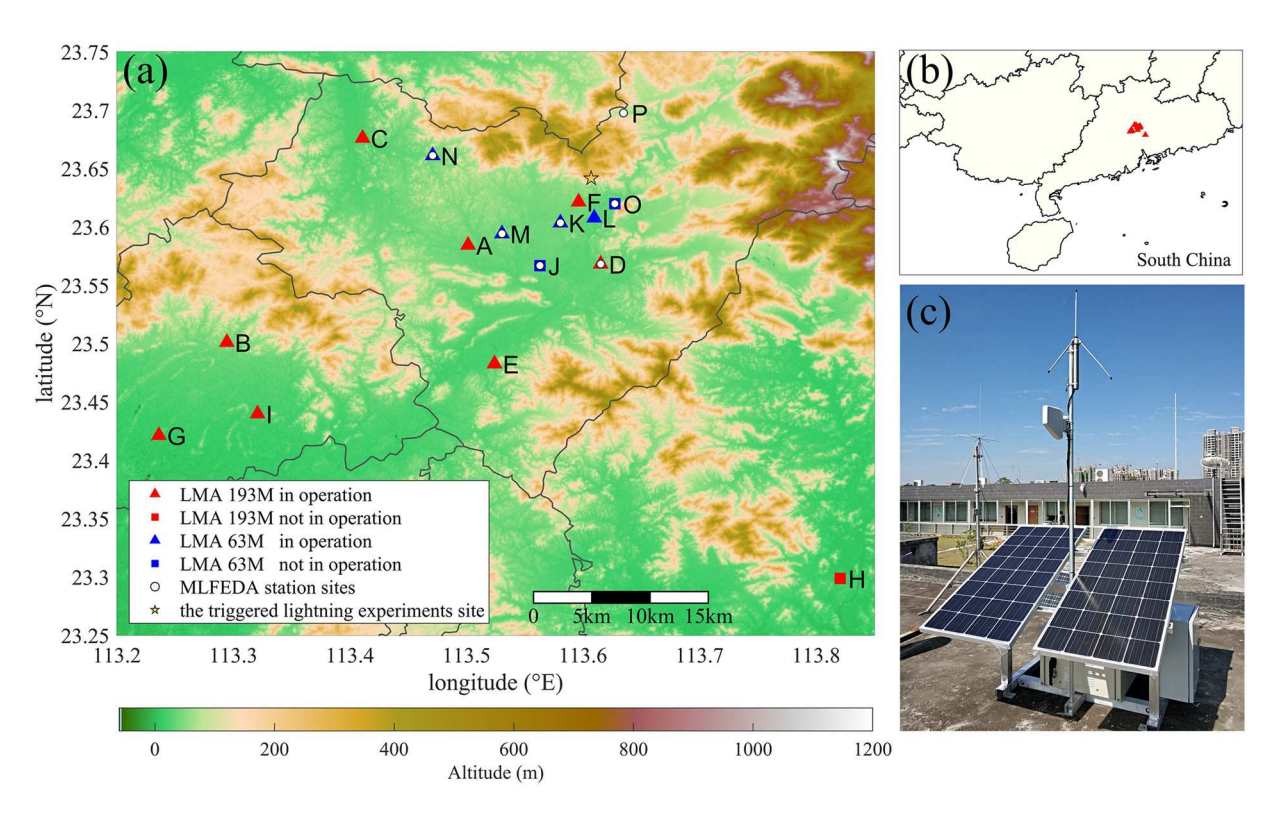


Figure 1. (a) The station locations of Guangdong Lightning Mapping Array (GDLMA) and Low-to-Mid Frequency E-field Detection Array (MLFEDA). (b) The location of the GDLMA network in South China. (c) Exterior view of a GDLMA substation. Red markers (A–I) indicate GDLMA stations with a center frequency of 193 MHz, blue markers (J–O) indicate stations with a center frequency of 63 MHz, and white scatters (D, J, K, M, O, P) indicate MLFEDA stations. The triangular markers indicate the operational stations and the square markers indicate stations that were not in operation in 2021. The star marker indicates the location of the triggered lightning experiments site.

#### 2.2. MLFEDA

MLFEDA is an upgraded station network of Low-frequency E-field Detection Array (LFEDA) (Chen et al., 2019; Shi et al., 2017; Zhang et al., 2022), operating in low-to-mid frequency bands (10 k–1 M). It was established in Conghua, Guangzhou by the lightning detection group of CAMS in 2021. Compared to previous LFEDA, the new array utilizes FPGA technology with lower power consumption (20–25 W) and real-time processing speed (10 pulses/100 µs). It has enhanced capabilities for capturing discharge pulse signals, allowing for a higher proportion of 3D lightning channel mapping. As shown in Figure 1a, the station location of MLFEDA is close to GDLMA. Both MLFEDA and GDLMA have 3D lightning positioning capabilities, allowing for a comparison of their positioning results.

# 2.3. Evaluation Methods

The location error is an important parameter and system metric that characterizes the performance of a lightning location system and can be evaluated using theoretical formulas, statistical simulations, and comparisons with results from different observation systems. The study of Koshak et al. (2004) suggested that the Monte Carlo simulation, which can test the actual TOA retrieval algorithm in the LMA positioning process, provides a more rigorous method for estimating errors and is suitable for detailed error analysis. Thomas et al. (2004) explained the network errors using a simple geometric model and the positioning results of aircraft tracks. The results were consistent with the calibration results of sounding balloon observations, demonstrating the reliability of these two methods. This study primarily focuses on evaluating positioning errors of GDLMA through Monte Carlo and theoretical statistics derived from an aircraft track location results. Additionally, the actual data of GDLMA are demonstrated by individual lightning discharges with different location errors and a brief analysis of a thunderstorm process.

ZHANG ET AL. 3 of 16

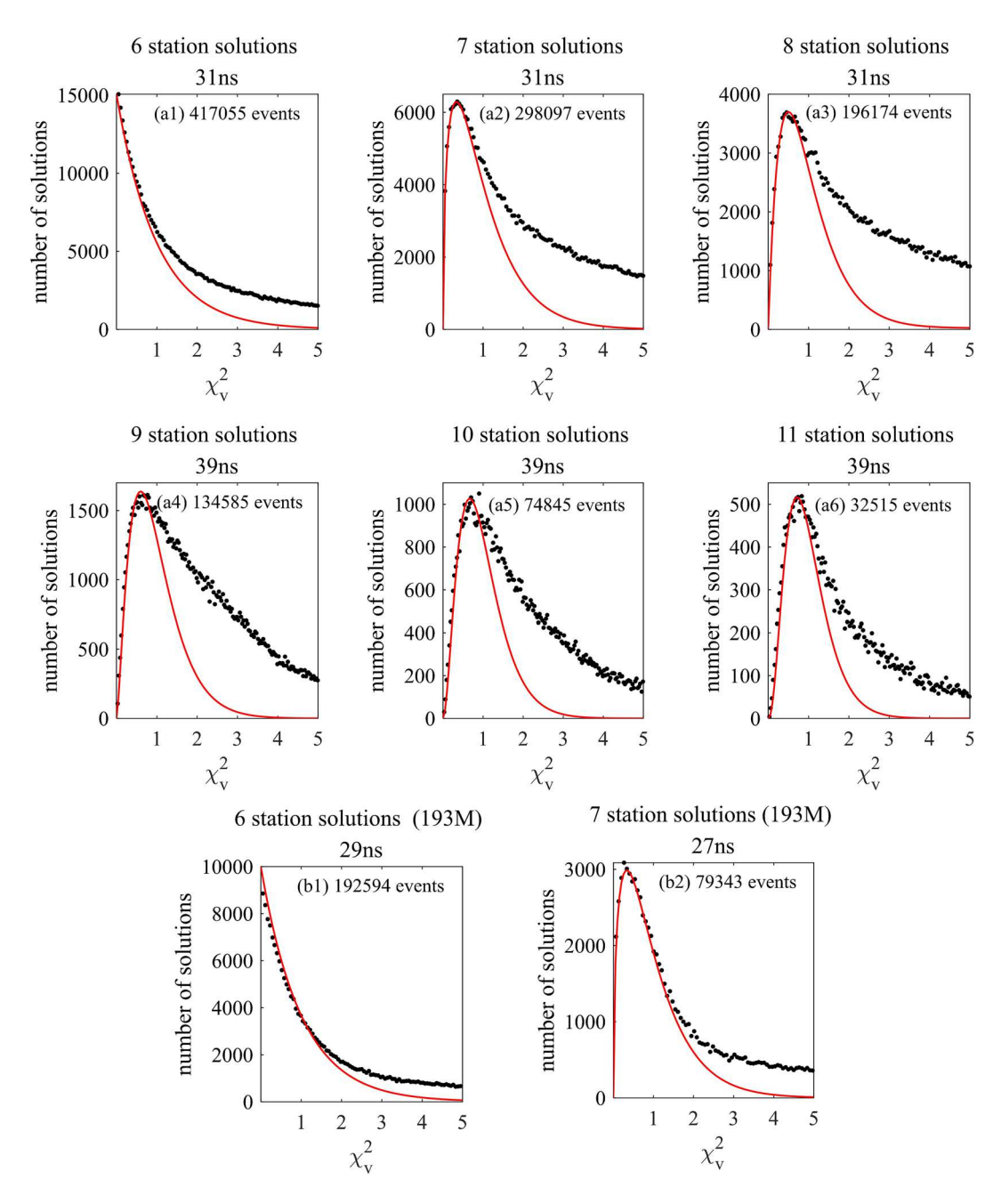


Figure 2. Adjusted  $\chi^2_{\nu}$  of Guangdong Lightning Mapping Array (GDLMA) data distributions (black) and theory  $\chi^2_{\nu}$  distributions (red) for different numbers of received stations. (a1–a6) GDLMA data with center frequencies of 193 and 63 MHz from 05:30 to 10:30 UTC on 6 August 2021. (b1 and b2) GDLMA data with a center frequency of 193 MHz from 17:40 to 18:30 UTC on 21 May 2020. The number of participating stations, number of events, and predicted timing errors are indicated in each panel.

# 3. Error Results and Analyses

# 3.1. Timing Errors

According to Equation 2, the location error is closely related to  $\Delta t_{\rm rms}$ . Therefore, the evaluation of  $\Delta t_{\rm rms}$  is conducted as a primary step. The effective  $\Delta t_{\rm rms}$  was estimated using actual observation lightning data of a thunderstorm in the Guangdong Province on 6 August 2021. According to the error adjustment equation  $\chi^2_{\rm v} = \chi^2_{\rm v_data} (70/\Delta t_{\rm rms})^2$ , real  $\Delta t_{\rm rms}$  can be determined by continuously adjusting  $\Delta t_{\rm rms}$  until the  $\chi^2_{\rm v}$  distribution closely matches the theoretical distribution. As shown in Figures 2a1–2a6, the estimated  $\Delta t_{\rm rms}$  were adjusted to 31 ns for 2–4 degrees of

ZHANG ET AL. 4 of 16

freedom, and 39 ns for 5–7 degrees of freedom. The overall average  $t_{\rm rms}$  is 35 ns, which represents a high level of timing precision.

It can be noticed that the  $\Delta t_{rms}$  is slightly larger when more stations participated in the solutions. Additionally, there are deviations between adjusted  $\chi_{\nu}^2$  distributions and theoretical distributions when  $\chi_{\nu}^2 > 1$ , indicating the presence of non-Gaussian errors. We speculate this discrepancy could be attributed to the utilization of two frequency bands in GDLMA, which results in phase differences and variations of peak arrival time in the waveforms. When more stations are involved in the computation, there may be a higher proportion of mixed-frequency band results, resulting in larger deviations from the theoretical distributions. By comparing the signal reception thresholds of the two frequency bands used in the data on the same day, 193 MHz (center frequency) stations had a lower reception threshold (averaging -91 dBm) compared to the 63 MHz stations (averaging -68 dBm), indicating a higher local noise floor for the latter. To verify the above speculation, the GDLMA data on 21 May 2020 (before the operation of the 63 MHz stations) was used to reassess the effective  $\Delta t_{rms}$ . Due to the limited number of stable and continuous running stations at the initial stage of GDLMA, the fitting results are provided only for 6 and 7 received stations, as shown in Figures 2b1 and 2b2. It can be observed that when operating only in the 193 MHz frequency band, the estimated  $t_{\rm rms}$  values are slightly smaller and  $\chi^2_{\rm v}$  distributions exhibit better alignment with theoretical distributions. It can be inferred that the utilization of mixed-frequency bands may contribute to the increased timing uncertainty in GDLMA. This is likely attributed to factors such as different local noise floors at the stations operating at different center frequencies, as well as variations in propagation speed and power attenuation.

#### 3.2. Monte Carlo Simulation Results

Location errors of GDLMA were estimated based on the modeling methods proposed by Koshak et al. (2004) and Chmielewski and Bruning (2016). A 3D grid was established with a horizontal grid spacing of 2.5 km. The grid covered 4–16 km MSL (mean sea level) and 400 km in the horizontal direction, with the center of GDLMA as the origin. Each subgrid contained 250 VHF-emitting point sources that underwent the LMA positioning algorithm, as shown in Equations 1 and 2. The simulation model took into account the station receiver threshold, center frequency, and source power to make the simulation results closer to the actual situation. A higher station receiver threshold, higher center frequency, and smaller simulated source power can reduce detection efficiency. The value of  $\Delta t_{rms}$  has a significant impact on the calculation results, with a smaller  $\Delta t_{rms}$  resulting in higher positioning accuracy. According to the result in Section 3.1, a random timing error from a normal distribution with a standard deviation of 35 ns was added to each simulated source arrival time. We used  $P^{-1}(P \in (0, 1,000) W^{-1})$  distribution described by Chmielewski and Bruning (2016) as the power distribution model for radiation sources.

The range (horizontal) error is expressed as  $\Delta r = \frac{\sum\limits_{i}^{k} \sqrt{(x_0 - \hat{x})^2 + (y_0 - \hat{y})^2}}{k}$ , and the altitude (vertical) error is expressed as  $\Delta z = \frac{\sum\limits_{i}^{n} (z_0 - \hat{z})}{k}$ , where  $(x_0, y_0, z_0)$  is the simulated values,  $(\hat{x}, \hat{y}, \hat{z})$  is the grid value, and k is the number of sources that meet the calculation requirements. In the calculation process, simulated sources with fewer than 6 received stations,  $\chi^2_v$  greater than 5, and those located below sea level were disregarded. Based on this data, we can determine the detection efficiency of radiation sources. As shown in Figure 3c, the detection efficiency exceeds 90% within a range of 100 km, and exceeds 99% within 50 km. It should be noted that the selection of different power distributions significantly affects the detection efficiency.

The spatial distribution of errors outside the station network exhibits noticeable directionality. As shown in Figures 3a and 3b, vertical errors are relatively small along the longest baseline (NE-SW) direction, while horizontal errors are smaller along the direction perpendicular to the longest baseline (NW-SE). Inside the network, horizontal errors are <18 m, and vertical errors are <50 m. At 100 km from the network center, horizontal errors in the longest baseline direction are <300 m, while in the perpendicular to the longest baseline direction, errors increase by about 3–4 times, showing significant directional variation. For vertical errors, this multiplier is around 2–3 times, smaller than that of horizontal errors. It can be explained by Equation 3, which is a theoretical model proposed by Thomas et al. (2004). The distance error outside the station network depends on the length of the baseline perpendicular to the direction of the source, while the altitude error depends on the parallel baseline. Although the longest baseline of GDLMA in the NE-SW direction is 43 km, it is only about 24 km in the NW-SE direction. Additionally, the horizontal error is slightly related to changes in altitude, but the vertical error

ZHANG ET AL. 5 of 16

2335084, 2023, 11, Downloaded from https://agupubs.onlinelibrary.wiley.com/doi/10.1029/2023EA003143 by New Mexico Institute Of Mining And Technology, Wiley Online Library on [1907/2024]. See the Terms and Conditions (https://onlinelibrary.

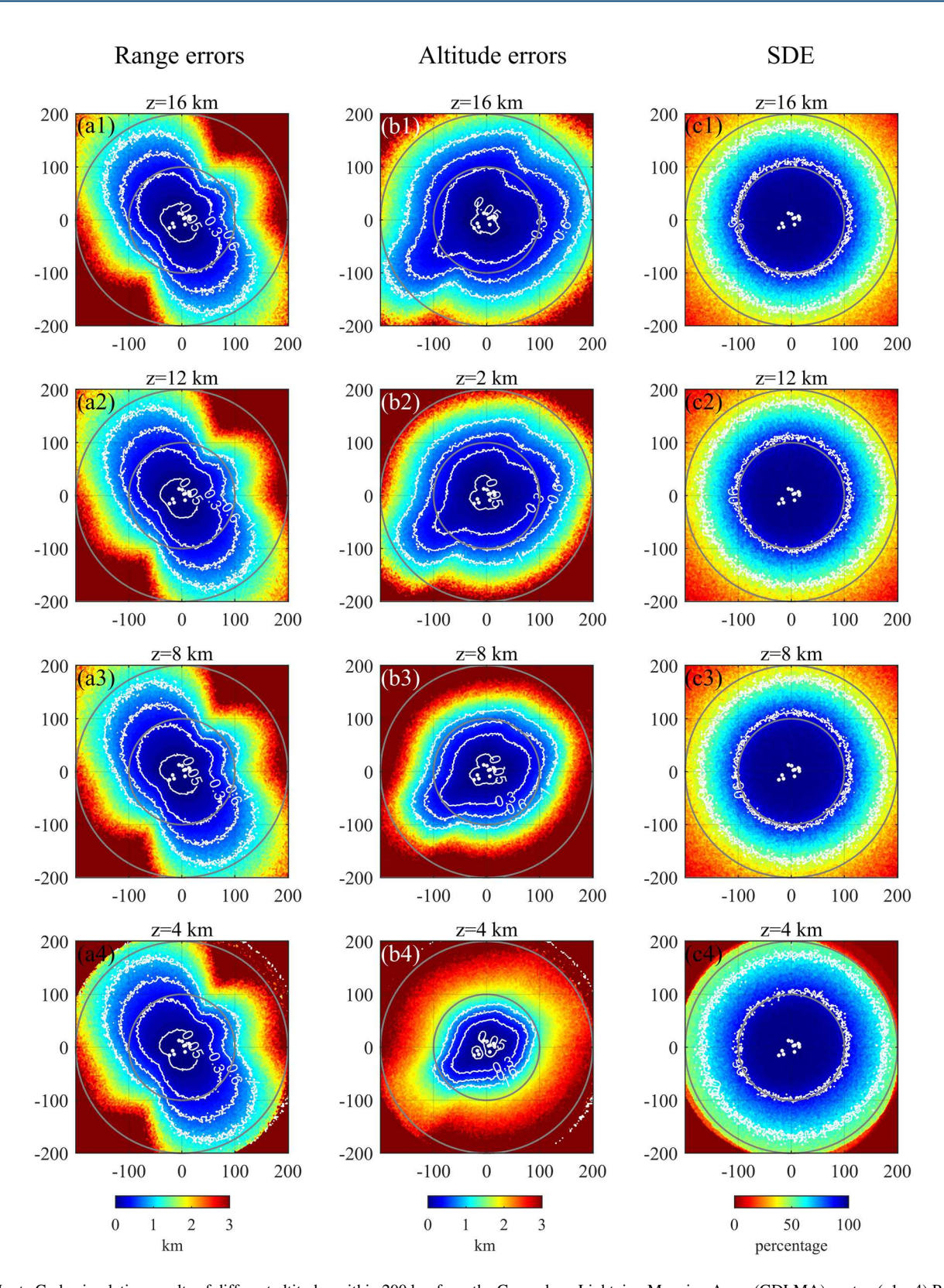


**Figure 3.** Monte Carlo simulation results of different altitudes within 200 km from the Guangdong Lightning Mapping Array (GDLMA) center. (a1–a4) Range errors at altitudes of 16, 12, 8, and 4 km, respectively. (b1–b4) Altitude errors. (c1–c4) Sources detection efficiency. White scatters indicate station locations and white lines are contour lines.

ZHANG ET AL. 6 of 16

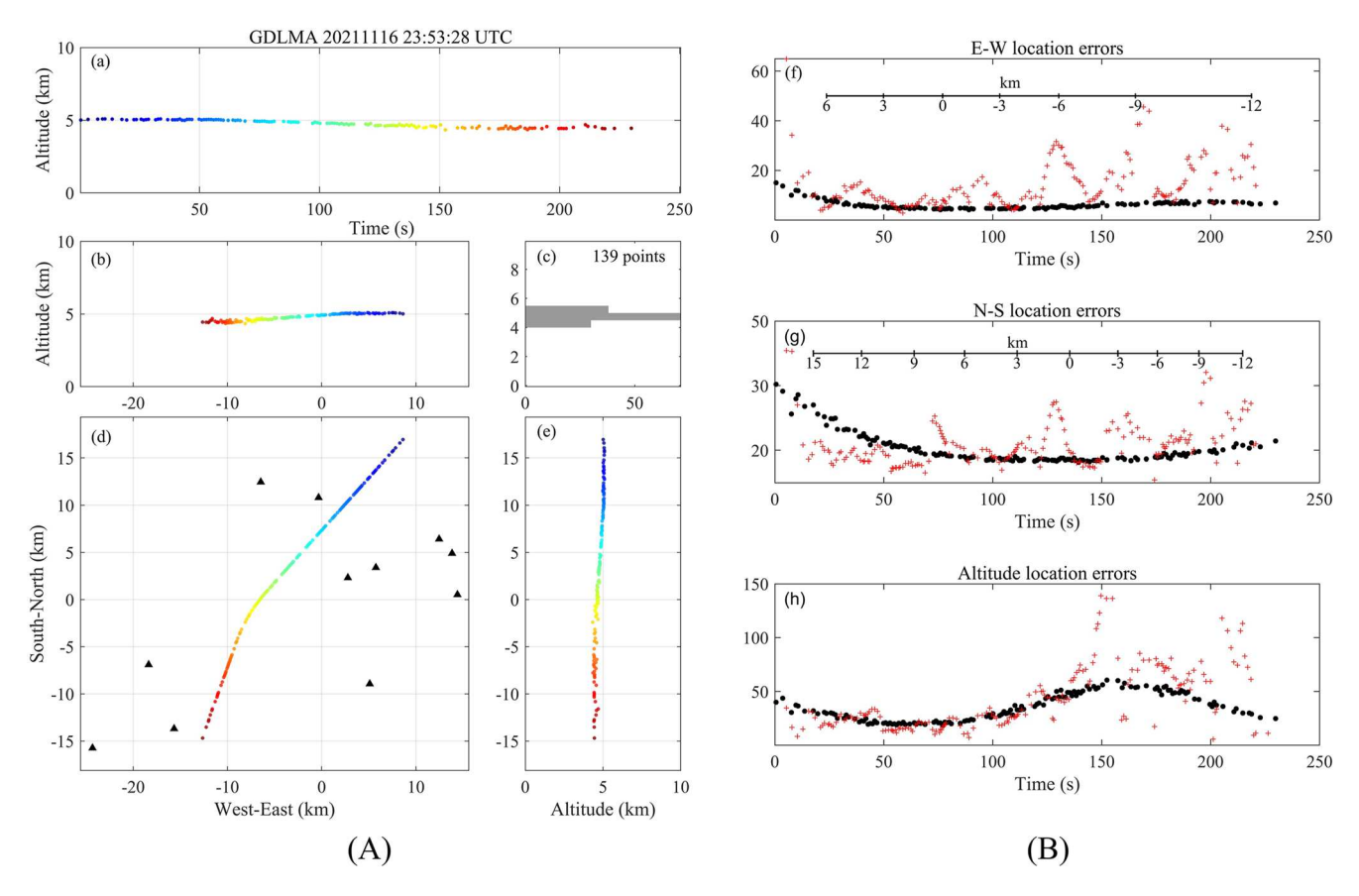


**Figure 4.** Plots of an aircraft track observed by Guangdong Lightning Mapping Array on 16 November 2021 (A) and location errors (B). (a–e) Altitude-time views and three different spatial projections, along with an altitude histogram of the number of sources. Colors represent time progression. (f–h) Standard variations (red) and Monte Caro simulation results (black) in W-E (x), S-N (y), and z directions.

at the same distance decreases with increasing altitude. In the simulation results, the difference in altitude errors at a distance of 100 km between 4 and 16 km MSL is  $\sim$ 3–5 times, with relatively smaller differences in the long baseline direction.

$$\begin{cases} \Delta r = 8 \left( \frac{r^2}{D^2} \right) c \Delta T \\ \Delta z = \left( \frac{r^2}{Dz} \right) c \Delta T \end{cases}$$
(3)

#### 3.3. Error Analysis Based on an Aircraft Track

During the flight of an aircraft, it can accumulate charges and emit a stable sequence of sparks under certain weather conditions. GDLMA is capable of tracking aircraft, and the detectability can indicate the sensitivity of the network. The source powers of the aircraft sparks are very low, just above the minimum detectable values of GDLMA. As the aircraft track is traceable and does not exhibit instantaneous large displacements, it is a good method for assessing the overall location errors of a network, apart from calibration equipment (Poehler, 1977; Thomas et al., 2004). Location errors can be analyzed by measuring the divergence of the positioning sources along the track.

As shown in Figure 4A, GDLMA detected the track of an aircraft on 16 November 2021 and located 139 radiation sources within 230 s. The initial position altitude was  $\sim$ 5.1 km MSL and gradually decreased to 4.4 km MSL along the southwest direction. Therefore, the track can be used to evaluate location errors over the network at altitudes of 4–5 km. The standard deviation of the scatter was determined relative to a polynomial fit to the track after data linearization and was smoothed by a 10 s (1.7 km) running average. The theoretical errors (Monte Carlo results) served as a comparison.

ZHANG ET AL. 7 of 16

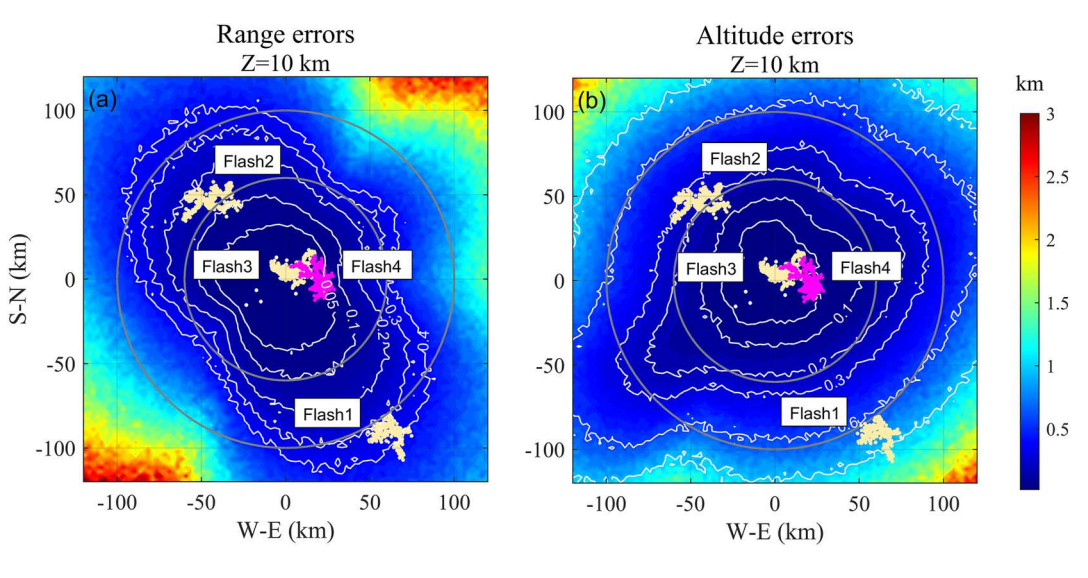


**Figure 5.** Four flash discharges at different distances from the station center overlain atop spatial plots of range errors (a) and altitude errors (b) at 10 km MSL. Flash 1–Flash 3 are shown in yellow and Flash 4 is shown in purple. White scatters indicate station locations and white lines are contour lines. The gray rings are 100 and 60 km from the center of Guangdong Lightning Mapping Array.

From Figure 4B, it can be observed that the distributions of standard deviation generally consist with theoretical errors. The standard deviations in the x and y directions are relatively small, with average errors of 14 and 12 m, respectively, and a total average horizontal error of 13 m. At 143 s, the aircraft made a turn when near the center of the station network, and both the standard deviation of altitude and theoretical vertical errors exhibited a peak. The overall average standard deviation in the z direction is around 41 m, and the fluctuation of standard deviation before the turn is significantly smaller than that after the turn. The fluctuation may be attributed to the accumulated error in the digital instrument clocks of each station during independent timing. The significant increase in altitude errors during the turning phase may be related to the descent in altitude and the distance of the nearest station. According to the geometric model provided by Thomas et al. (2004), the altitude positioning accuracy over the network is primarily determined by the closest station to the radiation source. There is a region within the GDLMA network where the vertical error slightly increases at the same altitude. Overall, the consistency between the standard deviations and theoretical errors indicates that the simulation results are reliable and can be used as a reference.

#### 4. GDLMA Detection Results

#### 4.1. Flash Examples

As shown in Figure 5, four lightning flashes (Flash 1–Flash 4) with different distances from the network are presented to demonstrate the location results that vary with different location errors. Flash 1 occurred 100 km away from the GDLMA center, with horizontal errors of 0.3–0.4 km and vertical errors of 0.6–1 km. As shown in Figure 6A, the location results are relatively dispersed, but a basic structure can be observed. It has a duration of 270 ms and a convex hull area of 426 km². Considering that VHF radiations from the positive charge region are more likely to be detected after long-distance propagation, the altitude distribution of radiation sources tends to be unimodal, corresponding to the positive charge region. Assuming that the altitude range of the charge region corresponds to the half-peak width of the altitude distribution, the inferred positive charge region of Flash 1 is between 8.3 and 9.8 km MSL. It should be noted that location results of distant lightning flash may lead to underestimated coverage area and overestimated altitude, due to increased location errors (Fuchs et al., 2016; Thomas et al., 2004).

As the distance decreases, the mapping results of lightning become more accurate and clear. As shown in Figure 6B, Flash 2 occurred  $\sim$ 65 km away from the network center, with horizontal errors of 0.1–0.2 km and vertical errors of 0.1–0.3 km. It has a duration of 440 ms and a convex hull area of 589 km², and the inferred positive charge region is at an altitude of 9.3–10.8 km MSL. Compared to Flash 1, location errors of Flash 2 have decreased by more than half, resulting in a more compact flash channel structure. This also indicates that lightning discharges within location errors of 300 m can be effectively captured and mapped.

ZHANG ET AL. 8 of 16

com/doi/10.1029/2023EA003143 by New Mexico Institute Of Mining And Technology, Wiley Online Library on [19/07/2024]. See the Term

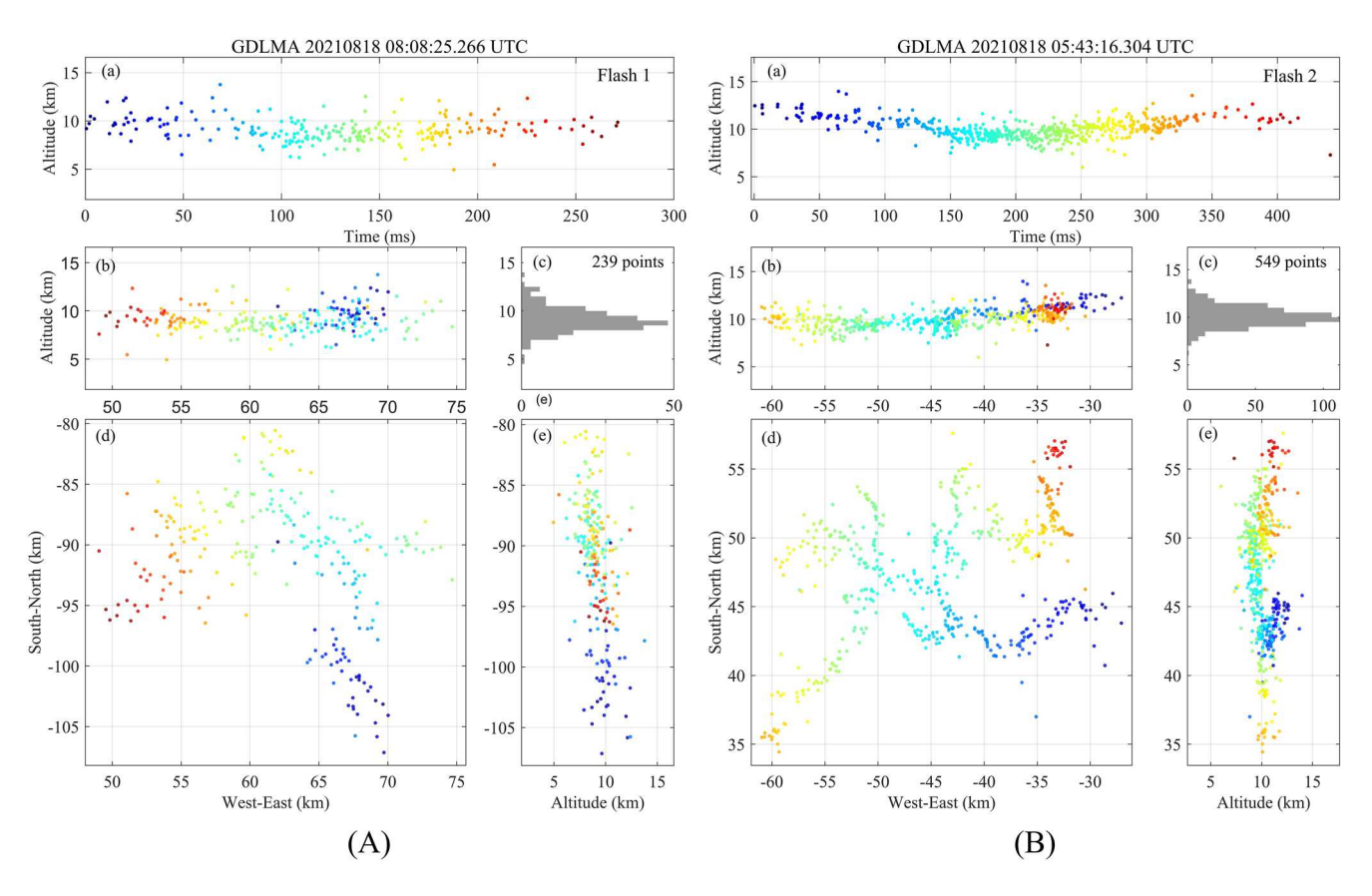


Figure 6. Mapping results of Flash 1 (A) and Flash 2 (B) produced by Guangdong Lightning Mapping Array. (a) Altitude-time views. (b) West-East vertical projections. (c) Histogram of radiation source altitudes. (d) Plan views. (e) South-North vertical projections. Sources located by six or more stations and  $\chi_v^2 < 1$  are shown.

Flash 3 and Flash 4 are shown in Figures 7A and 8A, respectively. They occurred over or near the network, with horizontal and vertical errors both within 50 m. Flash 3 has a duration of 612 ms and a convex hull area of 364 km<sup>2</sup>. Due to smaller location errors, clearer lightning flash branching structures were obtained. It exhibited a dipole structure, with the inferred upper positive charge region and the inferred negative charge region distributed at altitudes of 8–10.5 and 4.5–5.5 km, respectively. It initiated at an altitude of 6.7 km, with a clear negative upward leader propagated toward the upper positive charge region and transitioned to horizontal propagation at 10 km MSL at 17 ms. At the same time, GDLMA sources started to appear in the lower negative charge region. After 248 ms, radiation sources of the upper positive charge region ceased to be located, while sources of the lower negative charge region continued.

Flash 4 is a multistroke negative cloud-to-ground (CG) flash with a duration of 1.56 s and a convex hull area of 405 km². The inferred negative charge region is at 5–7 km MSL. The first radiation appeared at an altitude of 13.8 km and discharged toward the ground after a brief intracloud process at 54 ms. Based on the fast electric field change waveforms shown in panel (w) of Figure 8B, it is confirmed that Flash 4 consisted of 6 return strokes (RSs), with the first three (RS1–RS3) corresponding to stepped leaders and the last three (RS4–RS6) corresponding to dart leaders. The strike positions of RS1–RS3 were different, while RS4–RS6 had the same grounding position as RS3. GDLMA successfully located the first three clear downward negative stepped leaders, demonstrating its ability to locate low-altitude discharges near the station network.

# 4.2. Comparison of Mapping Results

# 4.2.1. Differences in Overall Positioning Results

With the improvement of location technique and hardware upgrades, a number of lightning location systems operating in the LF frequency band have also demonstrated the ability to depict 3D lightning channels and show an overall structure resemblance to the results of LMA (Bitzer et al., 2013; Lyu et al., 2014; Wu et al., 2018;

ZHANG ET AL. 9 of 16

onlinelibrary.wiley.com/doi/10.1029/2023EA003143 by New Mexico Institute Of Mining And Technology, Wiley Online Library on [1907/2024]. See the Terms

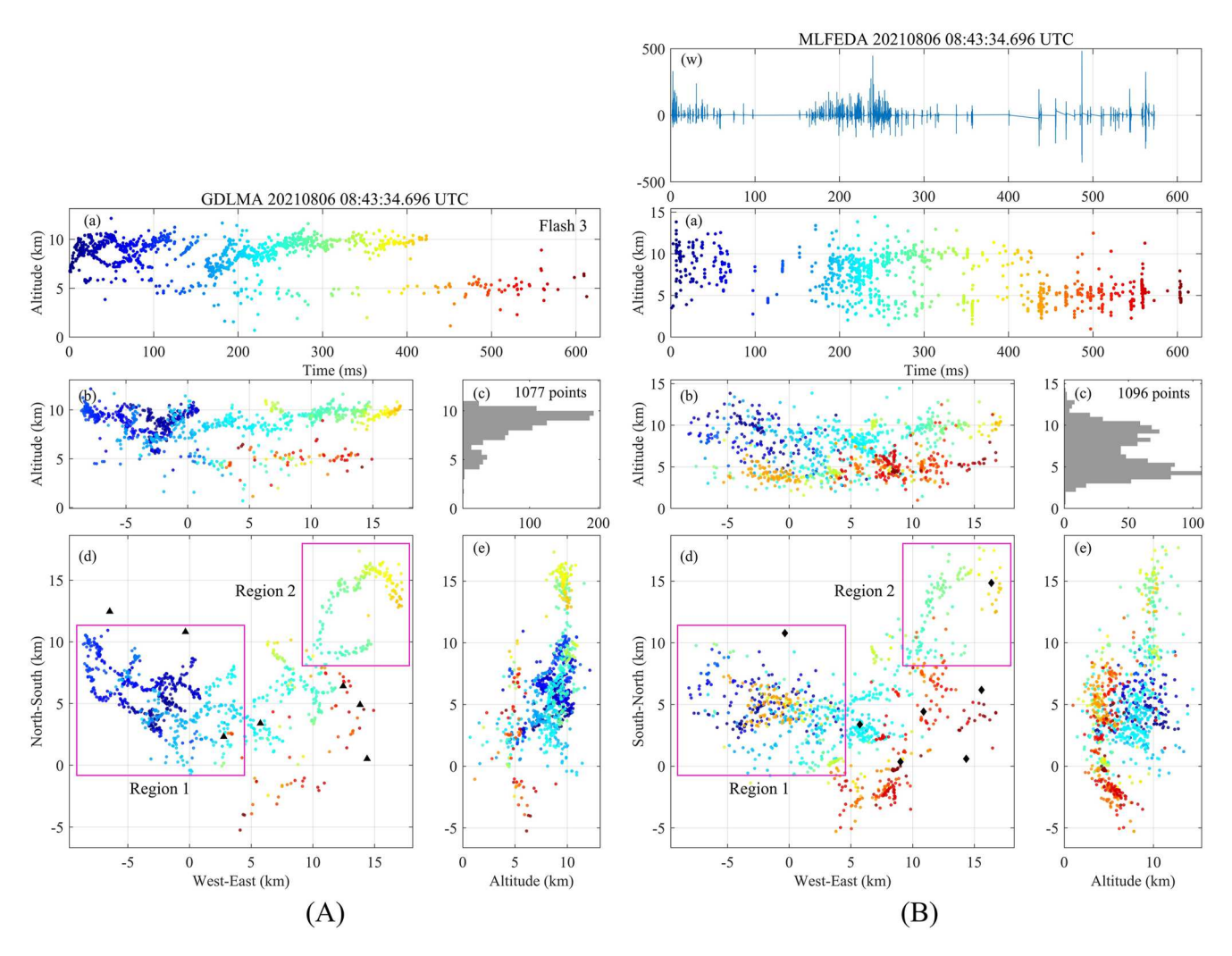


Figure 7. Mapping results of Flash 3 produced by Guangdong Lightning Mapping Array (GDLMA) (A) and Low-to-Mid Frequency E-field Detection Array (MLFEDA) (B). (a) Altitude-time views. (b) West-East vertical projections. (c) Histogram of radiation source altitudes. (d) Plan views. (e) South-North vertical projections. (w) Fast electric field change waveforms. The black triangle marks in A(d) indicate GDLMA stations and the black square marks in B(d) indicate MLFEDA stations. The center of GDLMA is taken as the coordinate origin of both (A) and (B). GDLMA sources located by six or more stations and  $\chi_v^2 < 1$ , and MLFEDA sources located by four or more stations and  $\chi_v^2 < 0.1$  are shown.

Zhang et al., 2022; Zhu et al., 2020). However, the mapping location results by the LF system and VHF system are often not matched due to differences in frequency bands and location techniques (Zhu et al., 2020). We are also interested in the similarities and differences between the two lightning location technologies. In this section, we present a brief comparison of the mapping results for Flash 3 and Flash 4 produced by GDLMA and MLFEDA.

The overall structure of lightning flashes mapped by GDLMA and MLFEDA are generally similar, as shown in Figures 7 and 8. For Flash 3, the flash duration time and convex hull area obtained by MLFEDA are 611.84 ms and 409 km², respectively, which are consistent with the results obtained by GDLMA but the area is slightly larger. The same applies to Flash 4, with a duration of 1.5 s and an area of 438 km² obtained by MLFEDA. However, due to the different physical processes corresponding to the VHF and LF frequency bands, there were some noticeable differences between them.

As shown in Figure 7d, the lightning channels mapped by GDLMA for Flash 3 are clearer and more continuous compared to the mapping results of MLFEDA, indicating that GDLMA exhibits superior channel characterization capability. This is mainly due to the frequent breakdown discharges involved in the formation and development of lightning channels, which generate VHF signals. On the other hand, LF signals mainly correspond to large transient current processes within preestablished channels, such as recoil streamer and K-process, which

ZHANG ET AL. 10 of 16

com/doi/10.1029/2023EA003143 by New Mexico Institute Of Mining And Technology, Wiley Online Library on [19/07/2024]. See the Terms

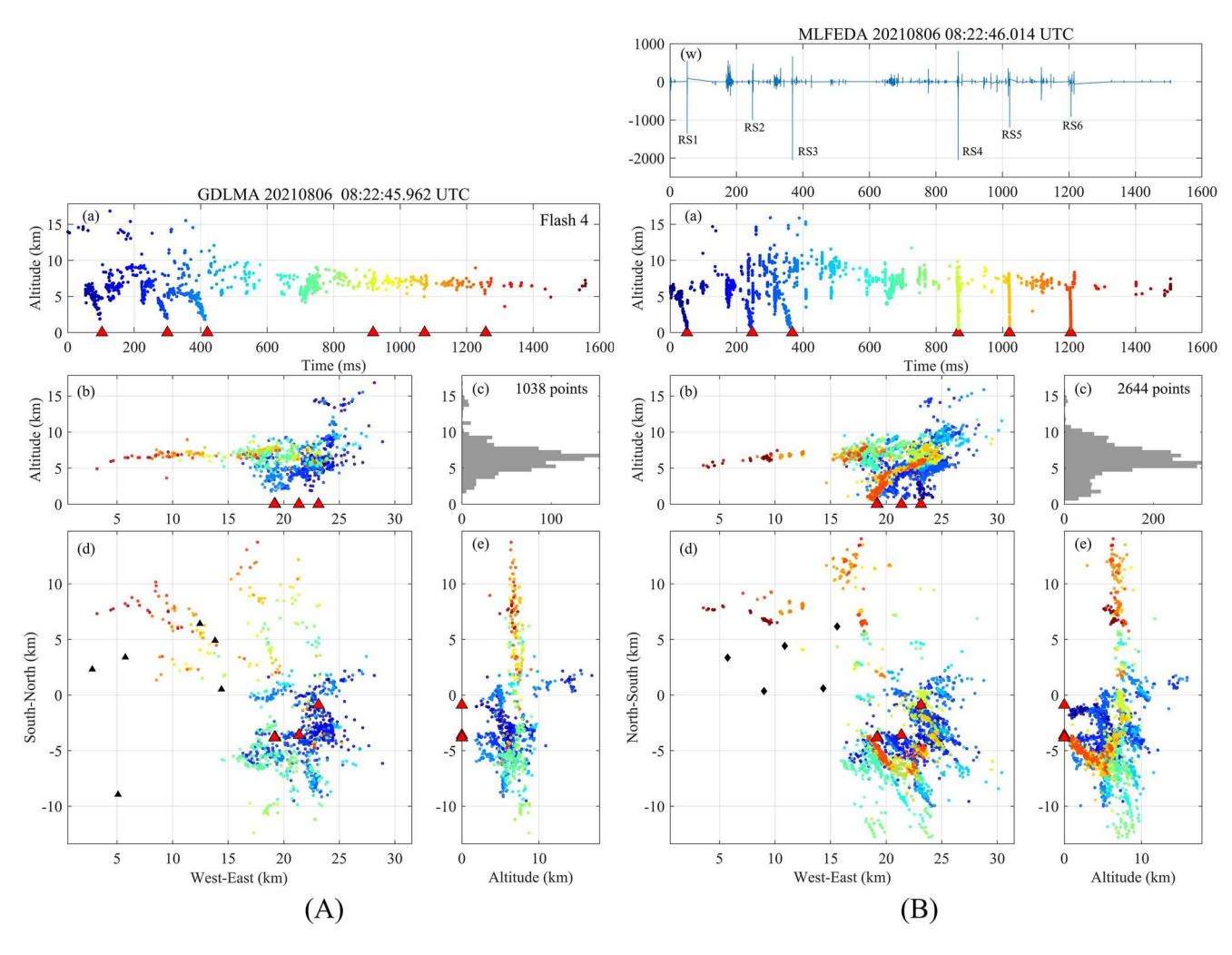


**Figure 8.** Mapping results of Flash 4 produced by Guangdong Lightning Mapping Array (GDLMA) (A) and Low-to-Mid Frequency E-field Detection Array (MLFEDA) (B). The plot layout is the same as in Figure 7, but shows MLFEDA sources located by five or more stations and  $\chi^2_{\nu} < 0.5$ . Flash 4 is a negative CG flash comprising six return strokes labeled as RS1–RS6 in (w). Red triangles indicate return stroke times and locations.

exhibit intermittent characteristics. Hence, it is challenging for MLFEDA to achieve continuous flash channel mapping results similar to GDLMA. Although MLFEDA sometimes located more radiation sources due to the differences in the technical window (80  $\mu$ s for GDLMA and minimum 10  $\mu$ s for MLFEDA), the lightning channel structure of intracloud flash and the intracloud portion of CG flash was still not as good as GDLMA.

When it comes to the downward leaders of CG flash, as shown in Figure 8, MLFEDA not only located the first three downward stepped leaders but also the subsequent three dart leaders, while GDLMA only located the first three. This is mainly due to dart leaders developing more rapidly and establishing themselves on existing channels, resulting in weak VHF signals. On the other hand, leader/RSs produce strong LF signals due to the large transient current process, which can be well located by MLFEDA. Additionally, MLFEDA located the downward leaders closer to the ground, while GDLMA ceased location at a height of 1–2 km above the ground. Furthermore, as shown in Region 1 of Figure 7d, MLFEDA captured some processes that GDLMA did not detect. Therefore, the combined use of GDLMA and MLFEDA can provide a more comprehensive understanding of the lightning discharge processes.

# 4.2.2. Differences in Details of Positioning Results

To further reveal the fundamental reasons for the differences between the two location results, a comparison at a microscopic level was conducted, focusing on individual discharge events. Fifty-one lightning flashes that occurred within the two networks on 6 August 2021 were selected for matching of VHF (GDLMA) and LF

ZHANG ET AL. 11 of 16

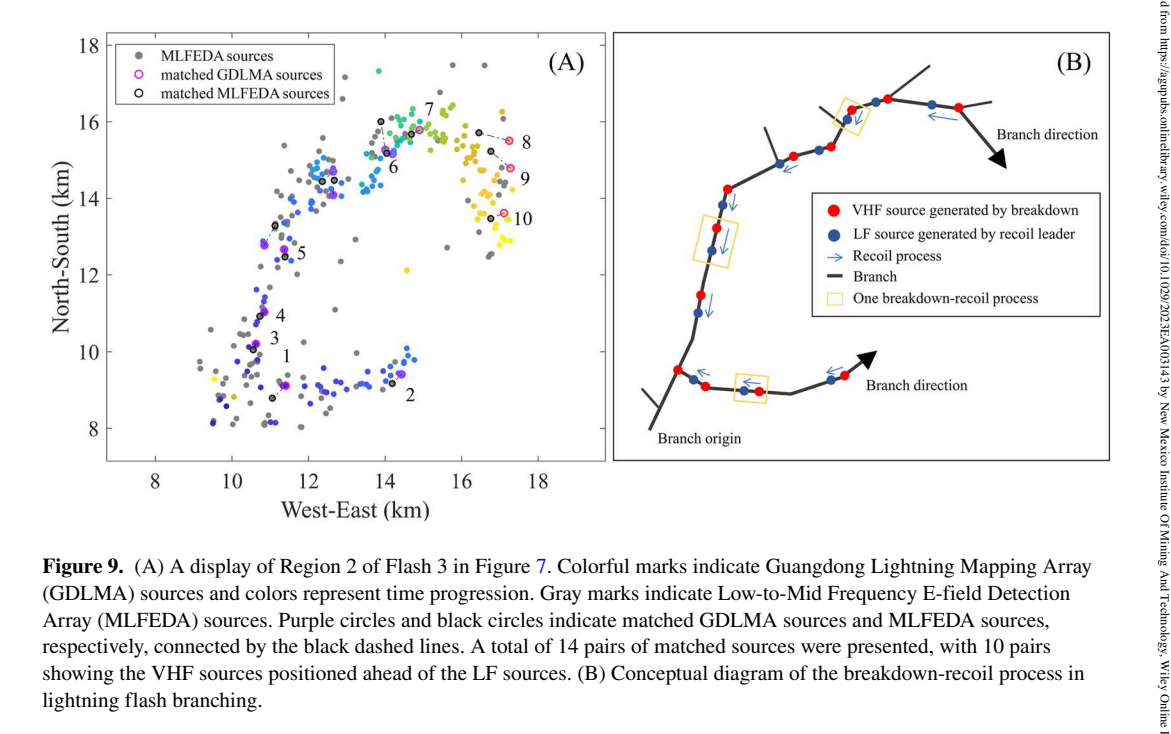


Figure 9. (A) A display of Region 2 of Flash 3 in Figure 7. Colorful marks indicate Guangdong Lightning Mapping Array (GDLMA) sources and colors represent time progression. Gray marks indicate Low-to-Mid Frequency E-field Detection Array (MLFEDA) sources, Purple circles and black circles indicate matched GDLMA sources and MLFEDA sources, respectively, connected by the black dashed lines. A total of 14 pairs of matched sources were presented, with 10 pairs showing the VHF sources positioned ahead of the LF sources. (B) Conceptual diagram of the breakdown-recoil process in lightning flash branching.

(MLFEDA) sources. LF sources were searched for matches within  $\pm 10 \,\mu s$  and 1 km radius of each VHF source. If one VHF source matched multiple LF sources, the LF source with the closest time was selected. In total, 796 pairs of sources were matched. The median and mean distances were 0.53 and 0.54 km, respectively. The median and mean time differences (absolute value) were 1.4 and 2.3 µs, respectively. Some studies have also compared the positions of radiation sources between VHF and LF location systems (Bitzer et al., 2013; Yoshida et al., 2014; Zhu et al., 2020), but the data provided exhibit statistical patterns without delving into one-to-one examination, hence not providing further explanations for the reasons behind the positional differences.

By comparing the matching results with the lightning channel, and statistically analyzing the relative positions of the matched VHF source and LF source, we found that the VHF source appeared more in front of the LF source in the direction of channel development. As an illustrative example, Figure 9A displays the channels and matching results in Region 2 of Flash 3 in Figure 7. This section encompassed 14 pairs of matched sources, with median and mean distances of 0.53 and 0.54 km, respectively. The median and mean time differences were 0.9 and 1.6 µs, respectively. Among these pairs, 10 (71%) VHF sources were ahead of LF sources in the direction of lightning channels.

Regarding the differences in the spatial positions of radiation sources between the two types of position results, a conceptual diagram is presented in Figure 9B to offer a speculative understanding of the underlying physical processes. The breakdown process occurs throughout the development of lightning channels, resulting in VHF signals. Each breakdown event may be accompanied by a recoil process, which rapidly develops backward from the leader's head along the original channel. Since the recoil activity occurs within the preexisting channel generally, it is more likely to correspond to charge transfer processes, producing LF signals. The spatial discrepancies in the position results between the two systems, as shown above, align with the latest understanding of lightning channel development. For instance, Zhang et al. (2017) found that each LF current signal corresponds to forward radiation breakdown and recoil processes when analyzing positive leader development. Additionally, Zhang et al. (2018) observed that LF signals are often associated with preceding abundant VHF position results when analyzing M-components.

For matched sources with different relative positions, they might be associated with alternative physical processes or could potentially result from matching errors arising from the limited temporal resolution of GDLMA and the location errors of the two systems. In reality, determining the relative positions of VHF sources and LF sources on small-scale lightning branches is challenging. Indeed, further analysis with higher-precision data is necessary. We intend to conduct more in-depth research by comparing the results from a higher-precision VHF continuous interferometer and the LF location system.

ZHANG ET AL. 12 of 16

om/doi/10.1029/2023EA003143 by New Mexico

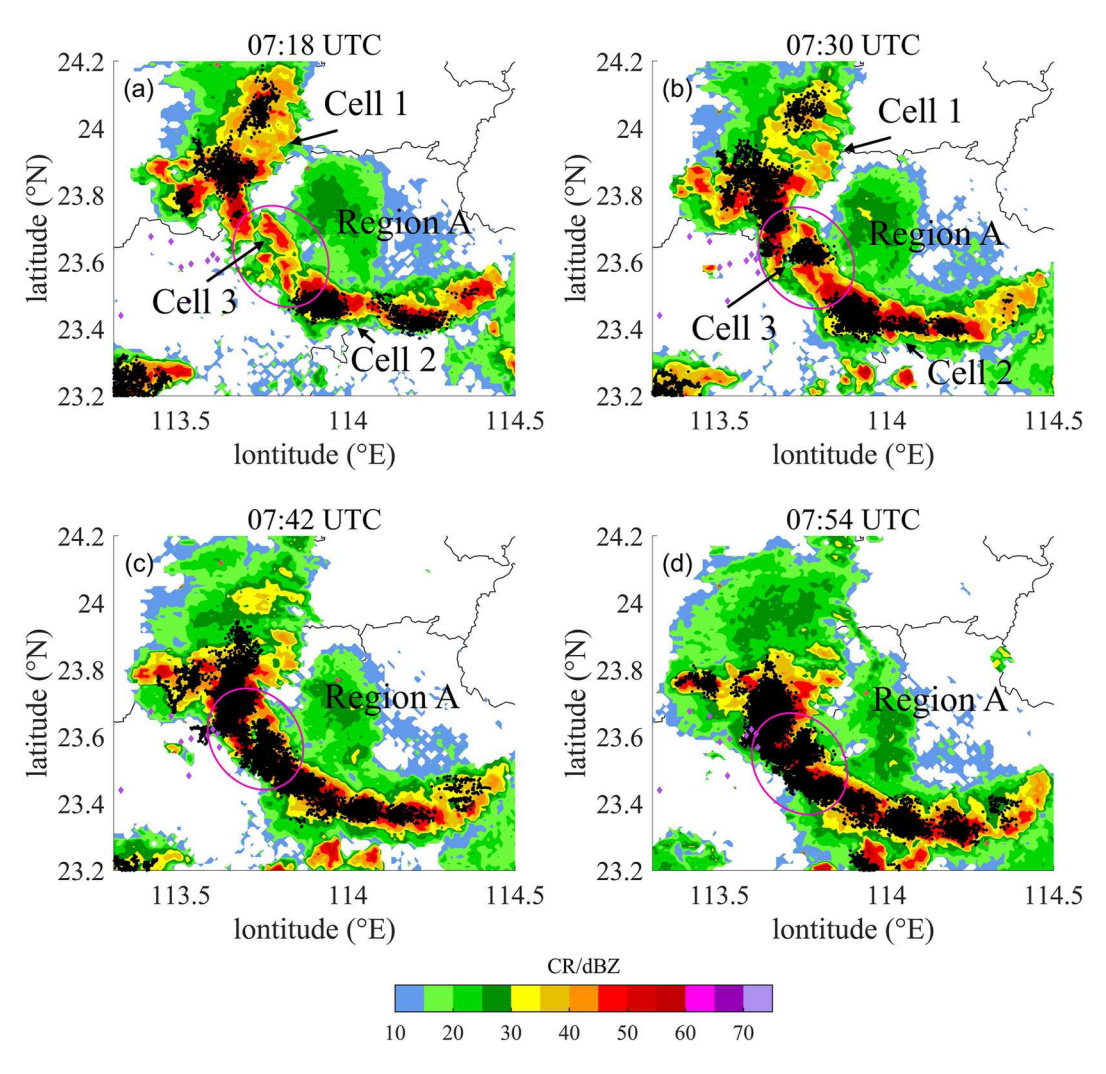


**Figure 10.** Corresponding Guangdong Lightning Mapping Array (GDLMA) sources for the merging of Cell 1 and Cell 2 on 6 August 2021 overlain radar composite reflectivity (CR) images. (a) 07:18 UTC. (b) 07:30 UTC. (c) 07:42 UTC. (d) 07:54 UTC. Black scatters indicate GDLMA radiation sources and purple marks indicate station locations. Region A indicates the region where the merging took place.

#### 4.3. A Thunderstorm Merging Process

In this section, a brief demonstration of the charge structure evolution during a merger process of two storm cells is presented. The Guangzhou S-band new generation Doppler weather radar data was used. The merger started at 07:30 UTC and finished at 08:00 UTC, taking place within a range of 50 km from the GDLMA. A squall line process is formed after the completion of merging. Throughout this process, the count of total flashes increased steadily and reached a peak after merging at 08:12 UTC (not shown).

As shown in Figure 10, the GDLMA sources are concentrated in the regions of strong radar reflectivity, and their positions and movements closely align, which demonstrates GDLMA's capability to indicate the development and evolution of thunderstorms. During the approach of Cell 1 and Cell 2, a new cell (Cell 3) emerged between them. It developed at a relatively lower altitude, and the first lightning radiation source appeared at 07:30 UTC. As shown in Figure 11A, Cell 1 and Cell 2 exhibited tripolar charge structures before merging, at altitudes of 11–14, 8–11, and 5–6 km, respectively. Cell 3 exhibited a dipolar charge structure at altitudes of 8–10 and 6–8 km, respectively. During the merging process, Cell 3 connected Cell 2 and Cell 1 sequentially, serving as a bridge between the two. Throughout the entire merging process, the merger region consistently maintained a relatively lower charge layer. After complete merging, a normal tripolar charge structure is observed.

ZHANG ET AL. 13 of 16

2335084, 2023, 11, Downloaded from https://agupubs.onlinelibrary.wiley.com/doi/10.1029/2023EA003143 by New Mexico Institute Of Mining And Technology, Wiley Online Library on [1907/2024]. See the Terms and Condition

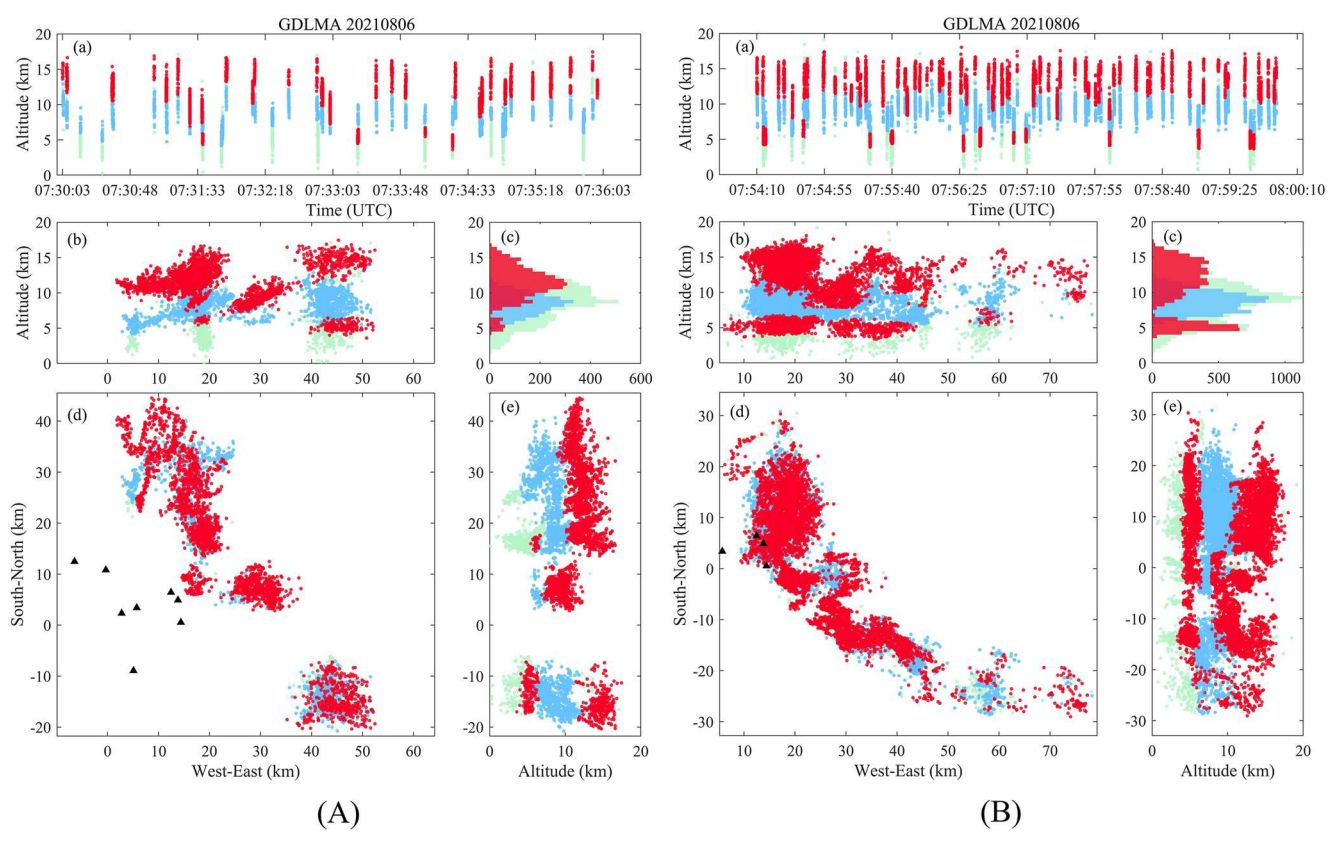


Figure 11. Charge structure distributions of Guangdong Lightning Mapping Array (GDLMA) sources during 07:30–07:36 UTC (A) and 07:54–08:00 UTC (B), corresponding to Figures 10b and 10d, respectively. (a–e) Altitude-time views and three different spatial projections, along with an altitude histogram of the number of sources. Red sources indicate inferred positive charge, blue sources indicate inferred negative charge and green sources indicate uncertain charge. Black triangles indicate GDLMA station locations.

#### 5. Conclusions

We evaluated the detection performance of GDLMA and demonstrated it through lightning flashes. The average timing uncertainty of GDLMA is 35 ns. As the number of participating stations increased to 9–11, the timing uncertainty slightly increased, possibly due to the combination of two receiving frequency bands, which introduces waveform differences and affects the calculation results. Through Monte Carlo, location errors are within 18 m horizontally and within 50 m vertically over the network, and exhibit significant directionality outside the network. Vertical errors are smaller in the longest baseline direction, while horizontal errors are smaller in the direction perpendicular to the longest baseline. The directional difference in horizontal error is greater than that of the vertical error. Horizontal errors are little related to altitude variations, but vertical errors at the same distance decrease with increasing altitude. Based on the aircraft track, the average horizontal error is 13 m and the average vertical error is 41 m at an altitude of 4–5 km over the network, following a similar trend to theoretical errors and indicating the usability of the simulation results.

Location results under different error ranges were demonstrated. In the range with location errors of 0.3–0.4 km horizontally and 0.6–1 km vertically at a distance of 100 km from the station network center, the lightning mapping results were scattered, but the basic lightning flash structure and characteristics such as positive charge region altitude and coverage area can still be obtained. In the range of location errors of 0.1–0.2 km horizontally and 0.1–0.3 km vertically at a distance of  $\sim$ 65 km, clearer and more continuous lightning channels could be obtained. With location errors within 50 m near the station network, multipolar charge structures and clearer lightning channel structures can be revealed.

Although the location results of GDLMA and MLFEDA showed similarities in overall structure and spatial distribution, GDLMA was capable of depicting clearer and more continuous lightning channels in intracloud flash

ZHANG ET AL. 14 of 16

Acknowledgments

2021Z011).

This research was funded by the

National Key Research and Development

Program of China (2017YFC1501501,

Fund of CAMS (2023KJ050), and the

Basic Research Fund of Chinese Acad-

emy of Meteorological Sciences (Grant

2019YFC1510103), S&T Development

and the intracloud portion of CG flash, while MLFEDA was better at locating dart leaders and K-processes. This reveals their complementarity to some extent. In addition, by comparing the spatial positions of matched VHF and LF sources along the lightning channel, it was observed that VHF sources were more located ahead of the LF sources in the lightning channel development direction. In this situation, it may be due to the small-scale recoil process that accompanies the breakdown process. Different frequency bands correspond to different physical processes, and their combined use will provide more comprehensive lightning information.

According to the inferred multicell thunderstorm charge structure from GDLMA, a weaker dipole structure cell formed as a connecting bridge between two equally intense tripolar structure cells before their merging. Throughout the entire merging process, the merger region consistently maintained a relatively lower charge layer. The completion of merging resulted in a squall line, exhibiting a normal tripolar charge structure.

# **Data Availability Statement**

The data used in this work are available at https://doi.org/10.5281/zenodo.8353398 (Zhang et al., 2023).

#### References

- Barth, M. C., Cantrell, C. A., Brune, W. H., Rutledge, S. A., Crawford, J. H., Huntrieser, H., et al. (2015). The Deep Convective Clouds and Chemistry (DC3) field campaign. Bulletin of the American Meteorological Society, 96(8), 1281–1309. https://doi.org/10.1175/BAMS-D-13-00290.1
- Bitzer, P. M., Christian, H. J., Stewart, M., Burchfield, J., Podgorny, S., Corredor, D., et al. (2013). Characterization and applications of VLF/LF source locations from lightning using the Huntsville Alabama Marx Meter Array. *Journal of Geophysical Research: Atmospheres*, 118, 3120–3138. https://doi.org/10.1002/jgrd.50271
- Bruning, E. C., & MacGorman, D. R. (2013). Theory and observations of controls on lightning flash size spectra. *Journal of the Atmospheric Sciences*, 70(12), 4012–4029. https://doi.org/10.1175/JAS-D-12-0289.1
- Carey, L. D., Koshak, W., Peterson, H., & Mecikalski, R. M. (2016). The kinematic and microphysical control of lightning rate, extent, and NOX production. *Journal of Geophysical Research: Atmospheres*, 121, 7975–7989. https://doi.org/10.1002/2015JD024703
- Chen, Z., Zhang, Y., Zheng, D., Zhang, Y., Fan, X., Fan, Y., et al. (2019). A method of three-dimensional location for LFEDA combining the time of arrival method and the time reversal technique. *Journal of Geophysical Research: Atmospheres*, 124, 6484–6500. https://doi.org/10.1029/2019JD030401
- Chmielewski, V. C., & Bruning, E. C. (2016). Lightning Mapping Array flash detection performance with variable receiver thresholds. *Journal of Geophysical Research: Atmospheres*, 121, 8600–8614. https://doi.org/10.1002/2016JD025159
- Cullen, M. R. (2013). The Houston Lightning Mapping Array: Network installation and preliminary analysis. Retrieved from https://oaktrust.library.tamu.edu/handle/1969.1/151109
- Davis, T. C., Rutledge, S. A., & Fuchs, B. R. (2019). Lightning location, NOx production, and transport by anomalous and normal polarity thun-derstorms. *Journal of Geophysical Research: Atmospheres*, 124, 8722–8742. https://doi.org/10.1029/2018JD029979
- Fuchs, B. R., Bruning, E. C., Rutledge, S. A., Carey, L. D., Krehbiel, P. R., & Rison, W. (2016). Climatological analyses of LMA data with an open-source lightning flash-clustering algorithm. *Journal of Geophysical Research: Atmospheres*, 121, 8625–8648. https://doi. org/10.1002/2015JD024663
- Koshak, W., Solakiewicz, R., Blakeslee, R., Goodman, S., Christian, H., Hall, J., et al. (2004). North Alabama Lightning Mapping Array (LMA): VHF source retrieval algorithm and error analyses. *Journal of Atmospheric and Oceanic Technology*, 21(4), 543–558. https://doi.org/10.1175/1520-0426(2004)021<0543:NALMAL>2.0.CO;2
- Krehbiel, P. R., Thomas, R. J., Rison, W., Hamlin, T., Harlin, J., & Davis, M. (2000). GPS-based mapping system reveals lightning inside storms. Eos, Transactions American Geophysical Union, 81(3), 21–25. https://doi.org/10.1029/00EO00014
- Lang, T. J., & Rutledge, S. A. (2008). Kinematic, microphysical, and electrical aspects of an asymmetric bow-echo mesoscale convective system observed during STEPS 2000. *Journal of Geophysical Research*, 113, D08213. https://doi.org/10.1029/2006JD007709
- Lyu, F., Cummer, S. A., Solanki, R., Weinert, J., McTague, L., Katko, A., et al. (2014). A low-frequency near-field interferometric-TOA 3-D Lightning Mapping Array. Geophysical Research Letters, 41, 7777–7784. https://doi.org/10.1002/2014GL061963
- Pineda, N., Rigo, T., Montanya, J., & van der Velde, O. A. (2016). Charge structure analysis of a severe hailstorm with predominantly positive cloud-to-ground lightning. *Atmospheric Research*, 178, 31–44. https://doi.org/10.1016/j.atmosres.2016.03.010
- Poehler, D. H. A. (1977). An accuracy analysis of the LDAR system. NASA Contractor Report, CR-154631. Retrieved from https://ntrs.nasa.gov/citations/19790012317
- Rison, W., Thomas, R., Krehbiel, P., Hamlin, T., & Harlin, J. (1999). A GPS-based three-dimensional lightning mapping system: Initial observations in central New Mexico. *Geophysical Research Letters*, 26(23), 3573–3576. https://doi.org/10.1029/1999GL010856
- Rust, W., MacGorman, D., Bruning, E., Weiss, S., Krehbiel, P., Thomas, R., et al. (2005). Inverted-polarity electrical structures in thunderstorms in the Severe Thunderstorm Electrification and Precipitation Study (STEPS). *Atmospheric Research*, 76(1–4), 247–271. https://doi.org/10.1016/j.atmosres.2004.11.029
- Salvador, A., Pineda, N., Montanyà, J., López, J. A., & Solà, G. (2021). Thunderstorm charge structures favouring cloud-to-ground lightning. Atmospheric Research, 257, 105577. https://doi.org/10.1016/j.atmosres.2021.105577
- Shi, D., Zheng, D., Zhang, Y., Zhang, Y., Huang, Z., Lu, W., et al. (2017). Low-frequency E-field Detection Array (LFEDA)—Construction and preliminary results. Science China Earth Sciences, 60(10), 1896–1908. https://doi.org/10.1007/s11430-016-9093-9
- Souza, J. C. S., & Bruning, E. C. (2021). Assessment of turbulence intensity in different spots of lightning flash propagation. Geophysical Research Letters, 48, e2021GL095923. https://doi.org/10.1029/2021GL095923
- Tessendorf, S. A., Wiens, K. C., & Rutledge, S. A. (2007). Radar and lightning observations of the 3 June 2000 electrically inverted storm from STEPS. *Monthly Weather Review*, 135(11), 3665–3681. https://doi.org/10.1175/2006MWR1953.1
- Thomas, R., Krehbiel, P., Rison, W., Hunyady, S., Winn, W., Hamlin, T., & Harlin, J. (2004). Accuracy of the Lightning Mapping Array. *Journal of Geophysical Research*, 109, D14207. https://doi.org/10.1029/2004JD004549

ZHANG ET AL. 15 of 16

- Wiens, K. C., Rutledge, S. A., & Tessendorf, S. A. (2005). The 29 June 2000 supercell observed during STEPS. Part II: Lightning and charge structure. *Journal of the Atmospheric Sciences*, 62(12), 4151–4177. https://doi.org/10.1175/JAS3615.1
- Wu, T., Wang, D., & Takagi, N. (2018). Lightning mapping with an array of fast antennas. Geophysical Research Letters, 45, 3698–3705. https://doi.org/10.1002/2018GL077628
- Yoshida, S., Wu, T., Ushio, T., Kusunoki, K., & Nakamura, Y. (2014). Initial results of LF sensor network for lightning observation and characteristics of lightning emission in LF band. *Journal of Geophysical Research: Atmospheres*, 119, 12034–12051. https://doi.org/10.1002/2014JD022065
- Zhang, G., Li, Y., Wang, Y., Zhang, T., Wu, B., & Liu, Y. (2015). Experimental study on location accuracy of a 3D VHF lightning-radiation-source locating network. Science China Earth Sciences, 58(11), 2034–2048. https://doi.org/10.1007/s11430-015-5119-1
- Zhang, G., Wang, Y., Qie, X., Zhang, T., Zhao, Y., Li, Y., & Cao, D. (2010). Using lightning locating system based on time-of-arrival technique to study three-dimensional lightning discharge processes. Science China Earth Sciences, 53(4), 591–602. https://doi.org/10.1007/s11430-009-0116-x
- Zhang, H., Zhang, Y., Fan, Y., Zhang, Y., Krehbiel, P. R., & Lyu, W. (2023). Guangdong Lightning Mapping Array: Errors evaluation and preliminary results [Dataset]. Zenodo. https://doi.org/10.5281/zenodo.8353398
- Zhang, Y., Krehbiel, P. R., Zhang, Y., Lu, W., Zheng, D., Xu, L., & Huang, Z. (2017). Observations of the initial stage of a rocket-and-wire-triggered lightning discharge: Initial pulses of triggered lightning. *Geophysical Research Letters*, 44, 4332–4340. https://doi.org/10.1002/2017GL072843
- Zhang, Y., Zhang, Y., Zou, M., Wang, J., Li, Y., Tan, Y., et al. (2022). Advances in lightning monitoring and location technology research in China. *Remote Sensing*, 14(5), 1293. https://doi.org/10.3390/rs14051293
- Zhang, Y., Zhang, Y. J., Zheng, D., & Lu, W. (2018). Characteristics and discharge processes of M events with large current in triggered lightning. *Radio Science*, 53, 974–985. https://doi.org/10.1029/2018RS006552
- Zheng, D., Wang, D., Zhang, Y., Wu, T., & Takagi, N. (2019). Charge regions indicated by LMA lightning flashes in Hokuriku's winter thunder-storms. *Journal of Geophysical Research: Atmospheres*, 124, 7179–7206. https://doi.org/10.1029/2018JD030060
- Zhu, Y., Bitzer, P., Stewart, M., Podgorny, S., Corredor, D., Burchfield, J., et al. (2020). Huntsville Alabama Marx meter array 2: Upgrade and capability. Earth and Space Science, 7, e2020EA001111. https://doi.org/10.1029/2020EA001111

ZHANG ET AL. 16 of 16